AGU PUBLICATIONS

JGR

Journal of Geophysical Research: Oceans

RESEARCH ARTICLE

10.1002/2015JC011415

**Key Points:**
- Unique features of remote sensing reflectance in the UV wavelengths are measured in various waters
- The ocean color in the UV is particularly sensitive to the variation of spectral slope of the CDM
- Adding UV wavebands will significantly improve the retrieval of the spectral slopes for CDM

**Correspondence to:**
J. Wei,
jianwei.wei@umb.edu

**Citation:**
Wei, J., Z. Lee, M. Ondrusek, A. Mannino, M. Tzortziou, and R. Armstrong (2016), Spectral slopes of the absorption coefficient of colored dissolved and detrital material inverted from UV-visible remote sensing reflectance, *J. Geophys. Res. Oceans*, *121*, 1953–1969, doi:10.1002/2015JC011415.

Received 23 OCT 2015
Accepted 2 MAR 2016
Accepted article online 4 MAR 2016
Published online 26 MAR 2016



# Spectral slopes of the absorption coefficient of colored dissolved and detrital material inverted from UV-visible remote sensing reflectance

**Jianwei Wei[1], Zhongping Lee[1], Michael Ondrusek[2], Antonio Mannino[3], Maria Tzortziou[4], and Roy Armstrong[5]**

[1]Optical Oceanography Laboratory, School for the Environment, University of Massachusetts Boston, Boston, Massachusetts, USA, [2]NOAA/NESDIS Center for Weather and Climate Prediction, College Park, Maryland, USA, [3]Hydrospheric and Biospheric Sciences Laboratory, NASA Goddard Space Flight Center, Greenbelt, Maryland, USA, [4]Department of Earth and Atmospheric Science, The City College of New York, New York, New York, USA, [5]Bio-optical Oceanography Laboratory, University of Puerto Rico, Mayagüez, Puerto Rico, USA

**Abstract** The spectral slope of the absorption coefficient of colored dissolved and detrital material (CDM), $S_{cdm}$ (units: $nm^{-1}$), is an important optical parameter for characterizing the absorption spectral shape of CDM. Although highly variable in natural waters, in most remote sensing algorithms, this slope is either kept as a constant or empirically modeled with multiband ocean color in the visible domain. In this study, we explore the potential of semianalytically retrieving $S_{cdm}$ with added ocean color information in the ultraviolet (UV) range between 360 and 400 nm. Unique features of hyperspectral remote sensing reflectance in the UV-visible wavelengths (360–500 nm) have been observed in various waters across a range of coastal and open ocean environments. Our data and analyses indicate that ocean color in the UV domain is particularly sensitive to the variation of the CDM spectral slope. Here, we used a synthesized dataset to show that adding UV wavelengths to the ocean color measurements will improve the retrieval of $S_{cdm}$ from remote sensing reflectance considerably, while the spectral band settings of past and current satellite ocean color sensors cannot fully account for the spectral variation of remote sensing reflectance. Results of this effort support the concept to include UV wavelengths in the next generation of satellite ocean color sensors.

## 1. Introduction

The colored dissolved organic matter (CDOM) is an optically important and biogeochemically active component in the upper water column of the ocean. It is one of the major water constituents contributing to light attenuation in the ultraviolet (UV) and blue wavelengths [*Bricaud et al*., 1981], shielding the aquatic living system from damaging UV radiation [*Cullen and Neale*, 1994; *Lesser and Farrell*, 2004; *Shick et al*., 1996]. The CDOM originates from various sources including terrigenous inputs [*Wang et al*., 2004], coastal marshes [*Tzortziou et al*., 2008], mangrove forests [*Shank et al*., 2010], sediment resuspension [*Boss et al*., 2001], and plankton activities [*Nelson et al*., 2004; *Steinberg et al*., 2004]. Within the ocean, photochemical processes, microbial degradation as well as physical processes further regulate the amount, composition, and distribution of CDOM [*Conmy et al*., 2009; *Del Castillo and Miller*, 2011; *Hernes and Benner*, 2003; *Twardowski and Donaghay*, 2002]. Quantification and characterization of the CDOM absorption signature in surface waters is therefore critically important for understanding physical and biogeochemical processes in the marine environment.

The CDOM spectral absorption is typically approximated with an exponential decay function of wavelength from UV to visible [*Bricaud et al*., 1981; *Jerlov*, 1976]. Two parameters are essential in this model: one is the absorption coefficient at a reference wavelength (often at 440 nm) and the other one is the spectral slope, $S$ (units: $nm^{-1}$). Knowing the spectral slope, the CDOM absorption at the reference band can be readily extrapolated to other wavelengths. In the Northern Gulf of Mexico, *Carder et al*. [1989] observed that the CDOM spectral slope varies with the ratio of fulvic acids to humic acids. In more recent efforts, the spectral slopes were used as a tracer of the terrigenous dissolved organic carbon [*Del Castillo and Miller*, 2008; *Fichot and Benner*, 2012], wetland contributions [*Tzortziou et al*., 2008], aromatic content [*Chin et al*., 1994], and the

average molecular weight and photobleaching history of the dissolved organic carbon pool [*Helms et al*., 2008].

In ocean color remote sensing, because of their similar spectral shapes, CDOM, and the detrital material [*Roesler et al*., 1989] are often combined into one term, CDM, in the semianalytical inversion algorithms [*Carder et al*., 1991; *IOCCG*, 2006]. This is generally because the contribution of the detrital materials to the absorption coefficient is much less than that by CDOM, at least for oceanic waters. To retrieve CDM absorption coefficient from the ocean color, a priori assumptions are often needed to model the spectral slope of CDM absorption spectrum ($a_{cdm}$), $S_{cdm}$ (units: $nm^{-1}$). For example, the quasianalytical algorithm (QAA) empirically estimates $S_{cdm}$ from the ratio $R_{rs}(440)/R_{rs}(550)$ [*Lee et al*., 2009]. Another widely used algorithm, GSM, simply assumes $S_{cdm}$ as a constant globally [*Maritorena et al*., 2002]. Despite these simplifications, these algorithms have undoubtedly provided the opportunity for insights into the oceans with estimations of various optical components in various scales [*Lee et al*., 2010; *Matsuoka et al*., 2013; *Siegel et al*., 2002; *Zheng et al*., 2014]. In addition, two decades of satellite ocean color observations have led to great achievements in synoptic mapping of the combined absorption properties of CDOM and detritus in regional and global oceans [*Mannino et al*., 2014; *Nelson et al*., 2007; *Siegel et al*., 2005]. On the other hand, based on various field measurements, the CDOM absorption coefficients at a few selected wavelengths are often empirically modeled as functions of various $R_{rs}$ band ratios in different waters and the CDOM spectral slopes can be further determined from the empirically derived absorption coefficients [*D'Sa and Miller*, 2003; *Johannessen et al*., 2003; *Mannino et al*., 2008; *Pan et al*., 2008]. Recently, *Cao and Miller* [2015] proposed a new empirical algorithm for retrieving CDOM absorption spectral shape in the UV from visible ocean color bands, using a statistical approach and a training data set spanning a variety of water types.

Although past efforts have demonstrated success in estimating the component absorption of phytoplankton and CDM, there is a lack of analytical methodology for robust estimation of $S_{cdm}$ from satellite ocean color measurements. The current ocean color satellite sensors image the oceans with a limited number of visible bands, roughly centered at 412, 443, 490, 530, 550, and 670 nm. Several near-infrared (NIR) and/or shortwave infrared (SWIR) bands are used for atmospheric corrections [*Gordon and Wang*, 1994; *Wang et al*., 2009]. No operational ocean color satellite sensor measures ocean color at UV wavelengths. Recently, an inclusion of spectral bands in the UV has been proposed for the next generation of ocean color satellite sensors (e.g., PACE and GEO-CAPE) [*Del Castillo et al*., 2012; *Fishman et al*., 2012]. When the new sensors are in operation, there will be information available for the ocean color at UV bands.

This study represents the first effort of exploring the value of integrating UV measurements (360–400 nm) in the semianalytical inversion of $S_{cdm}$. The unique features in the hyperspectral remote sensing reflectance spectra in the UV and visible domain have been observed in various waters across a range of coastal and open ocean environments (section 2). The modeling results suggest that the observed spectral signature of remote sensing reflectance in the UV-visible domain is most likely resulted from variations of $S_{cdm}$ (could be either the spectral slope of CDOM or the spectral slope of the detrital materials, depending on which one dominates) (section 3). Our further analyses indicate that ocean color measurements including UV wavelengths will improve the retrieval of $S_{cdm}$, although the benefits on the accuracy of the retrieved phytoplankton absorption spectra are limited (section 4).

## 2. Background and Motivations

Ocean color is manifested by the remote sensing reflectance ($R_{rs}$, $sr^{-1}$), which is the ratio of water-leaving radiance ($L_w(0^+,\lambda)$) to downwelling plane irradiance just above the water surface ($E_d(0^+,\lambda)$). $R_{rs}$ is determined by the inherent optical properties (IOPs) [*Preisendorfer*, 1976] of water constituents, and often modeled as a simple function of the ratio of total backscattering ($b_b$) to absorption ($a$) coefficients [*Gordon et al*., 1988]

$$R_{rs}(\lambda) \propto \frac{b_b(\lambda)}{a(\lambda)+b_b(\lambda)} \tag{1}$$

For natural waters, the absorption coefficient ($a$, $m^{-1}$) is composed of the contributions of pure seawater ($a_w$, $m^{-1}$), phytoplankton ($a_{ph}$, $m^{-1}$), detritus ($a_{det}$, $m^{-1}$), and CDOM ($a_{cdom}$, $m^{-1}$), i.e., $a = a_w + a_{ph} + a_{det} + a_{cdom}$. The latter two components are usually summed together ($a_{cdm} = a_{det} + a_{cdom}$) since both detritus and CDOM absorption typically show an exponential increase with decreasing wavelength [*Roesler et al*.,

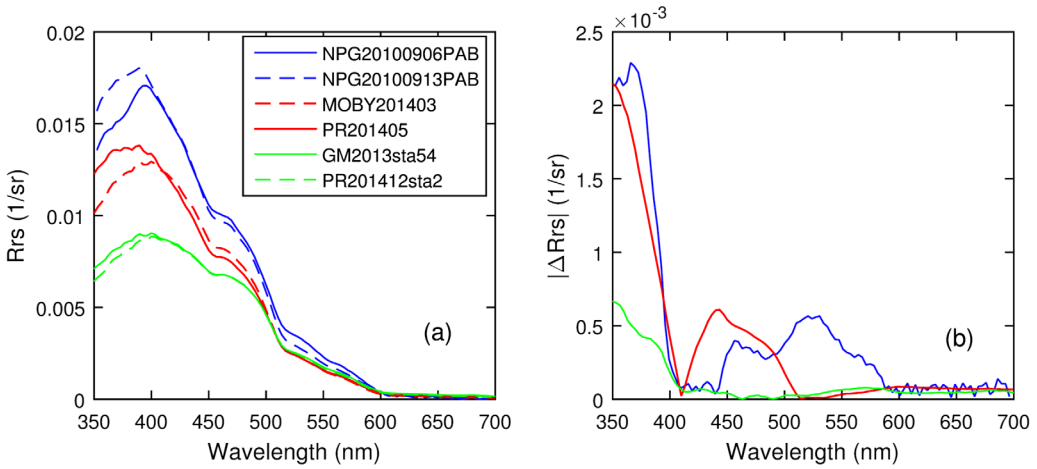


**Figure 1.** (a) Remote sensing reflectance measured in different oceanic waters. (b)Absolute difference between each paired $R_{rs}$ spectra.

1989] making it hard to separate mathematically from each other [*Carder et al*., 1999], at least in the visible bands. The nomenclature "detritus" is a practical simplification that combines nonalgal (or more accurately depigmented) particles into a single pool, but in reality represents a broad range of light-absorbing particles including inorganic sedimentary particles, organic particles of terrigenous or marine origin, and combinations of these. Similarly, the backscattering coefficient ($b_b$, $m^{-1}$) is practically decomposed into the contributions of pure seawater and particles, $b_{bw}$ and $b_{bp}$, respectively. The backscattering of particulates receives contributions from phytoplankton and detritus ($b_{bph}$ and $b_{bd}$). With a fundamental model like equation (1), significant efforts have been invested on the inversion of the IOPs from ocean color. Many semianalytical algorithms have been developed to retrieve spectral IOPs including total absorption and backscattering from $R_{rs}$ and further to partition the total absorption into corresponding constituents including $a_{ph}$ and $a_{cdm}$ [*IOCCG*, 2006; *Lee et al*., 2002; *Loisel and Stramski*, 2000; *Maritorena et al*., 2002; *Smyth et al*., 2006]. For the ocean color inversion algorithms, one general assumption is that the spectral shapes of water constituents are known. For example, the absorption of CDOM and detrital material in the UV and visible spectral range decrease in an exponential fashion with wavelength [*Carder et al*., 1991]

$$a_{cdm}(\lambda)=a_{cdm}(\lambda_0)\exp\left[-S_{cdm}\cdot(\lambda-\lambda_0)\right] \tag{2}$$

For the purposes of this study, the parameter $S_{cdm}$ represents the mean spectral slope between 360 and 700 nm. To further simplify, we ignored the dependence of $S_{cdm}$ in this spectral range [*Aurin and Mannino*, 2012; *Twardowski et al*., 2004]. The particle backscattering coefficient can be expressed by a power function [*Carder et al*., 1999; *Gordon and Morel*, 1983; *Lee et al*., 2002]

$$b_{bp}(\lambda)=b_{bp}(\lambda_0)\left[\frac{\lambda_0}{\lambda}\right]^{\eta} \tag{3}$$

where the exponent $\eta$ describes the shape of backscattering spectrum. Despite the fact that different semianalytical algorithms model $S_{cdm}$ and $\eta$ in slightly different ways [*Carder et al*., 1999; *Lee et al*., 2009; *Mouw et al*., 2013], they share a common goal that the $R_{rs}$ spectrum from the estimated IOPs should match spectrally the input $R_{rs}(\lambda)$.

Examples of remote sensing reflectance are given in Figure 1a, where three pairs of spectral $R_{rs}(\lambda)$ covering the UV-visible domain were measured in different oceanic waters and at different times (Table 1). The first pair of spectra (depicted in blue) was measured in the North Pacific Gyre (~300 km west of Hawaii) using a free-fall hyperspectral profiling radiometer (HyperPro, Satlantic Inc., Canada). For the profiling observations, $R_{rs}(\lambda)$ is determined as $R_{rs}(\lambda)=L_w(0^+,\lambda)/E_d(0^+,\lambda)$. $L_w(0^+,\lambda)$ is determined from the radiance right below the surface, $L_w(0^+,\lambda)=\tau\times L_u(0^-,\lambda)$, where the radiance transmittance $\tau$ is equal to 0.54 [*Austin*, 1974; *Wei et al*., 2015]. The second pair of $R_{rs}$ spectra was obtained at the Marine Optical Buoy (MOBY for short, located 10 km west of Lanai Island, Hawaii) and in the Caribbean Sea (south of La Parguera, Puerto Rico). The third

**Table 1.** Field Data of Remote Sensing Reflectance

| Pair # | Data _ID | Lat/Lon | Date/Time | Method[a] | Depth (m) | [CHL][b] (mg $m^{-3}$) |
|---|---|---|---|---|---|---|
| 1 | NPG20100906PAB | 17°31.1′N 157°23.3′W | 6 Sep 2009, 21:00 UTC | Depth profiling | 5000 | 0.05 |
| | NPG20100913PAB | 17°50.9′N 159°23.9′W | 13 Sep 2009, 21:10 UTC | Depth profiling | 5000 | 0.06 |
| 2 | MOBY201403 | 20°47.58′N 157°09.1′W | 4 Mar 2014, 22:46 UTC | SBA | 1200 | 0.08 |
| | PR201405 | 17°51.70′N 66°58.38′W | 3 May 2014, 16:31 UTC | SBA | 1000 | 0.10 |
| 3 | GM2013sta54 | 28°11.75′N 93°47.89′W | 15 Sep 2013, 14:49UTC | SBA | 70 | 0.20 |
| | PR201412sta2 | 17°54.36′N 66°58.32′W | 13 Dec 2014, 16:50UTC | SBA | 600 | 0.19 |

[a]The "Depth profiling" refers to the free-fall profiling measurement; "SBA" is the at-surface measurements using skylight-blocked approach.
[b]The chlorophyll a concentration is obtained from the MODIS Aqua monthly chlorophyll a product (http://oceancolor.gsfc.nasa.gov).

pair of data were measured in the northern Gulf of Mexico and a different station south of Puerto Rico. The latter two pairs of data were measured with the same instrument package based on the skylight-blocked approach [*Lee et al*., 2013], and the updated data processing procedures of *Wei et al*. [2015] were followed. Common and conspicuous features within each pair of spectra are that they retain almost the same spectral values in the visible domain (~410–700 nm). The absolute difference, $|\Delta R_{rs}(\lambda)|$, between each paired $R_{rs}$ in the visible domain is generally less than 0.0005 $sr^{-1}$ (Figure 1b). It is noted that these small differences are very close to the uncertainty of $R_{rs}$ from satellite ocean color sensors, which is reportedly ~0.0004 $sr^{-1}$ in the blue-green domain as estimated from MODIS-Aqua radiometric products over clear oceanic waters [*Gordon*, 1997; *Hu et al*., 2013]. The third pair of $R_{rs}$ shows a difference smaller than 0.0001 $sr^{-1}$ between 400 and 700 nm. In the UV domain, however, the $R_{rs}$ spectra within each pair diverge significantly from each other. The differences within each pair of $R_{rs}$ spectra reach up to 0.002 $sr^{-1}$, which is a factor of 4 compared to the difference in the visible domain. To our knowledge, such large contrasts of $R_{rs}$ in the UV-visible domain from field measurements have not been reported previously in the literature.

The current approaches of ocean color remote sensing retrievals rely on measurements at several visible wavelengths from 412 to 670 nm. For example, MODIS Aqua has wavelengths roughly centered at 412, 443, 490, 530, 550, and 670 nm, which does not have a possibility to capture the variability of the $R_{rs}$ spectrum in the UV domain as shown in Figure 1. The large differences in the $R_{rs}$ spectra in the UV spectral region shown in Figure 1 suggest that it could be highly due to the variability of the spectral slope of the CDM absorption coefficient, as the $R_{rs}$ spectra in the visible domain are almost the same for each pair. An immediate hypothesis follows: if a change in the spectral slope of CDM absorption coefficient can result in such differences in the $R_{rs}$ spectra in the UV but with no significant change in the visible (Figure 1), the models for $S_{cdm}$ based on $R_{rs}$ information in the visible bands [e.g., *Lee et al*., 2009] are insufficient and additional information in the UV would improve remote-sensing retrievals of $S_{cdm}$. The objective of this study is to investigate whether or not $R_{rs}$ data at UV wavelengths are a requisite for improved estimation of $S_{cdm}$ from ocean color remote sensing. Note that CDM itself is not a material, but a mathematical combination of the absorption properties of CDOM and detritus. Usually the CDOM absorption of oceanic waters in the 360–400 nm range is much stronger than the absorption by phytoplankton or detritus in this spectral range [*Bricaud et al*., 2010], the feature thus represents more of a contribution by CDOM, rather than the detritus.

## 3. Sensitivity of $R_{rs}$ Spectral Shapes to the Absorption and Scattering Properties

We systematically examined two types of oceanic waters to explore the sensitivity of the $R_{rs}$ spectral shapes to the variation of absorption and scattering properties. The first type represents hyperoligotrophic oceans with extremely low chlorophyll a concentration (0.07 mg $m^{-3}$). The second type is typical of higher chlorophyll concentration (0.15 mg $m^{-3}$), which is commonly seen in areas such as the equatorial upwelling regions, Southern Ocean and mid-high latitudes in the Northern Hemisphere. The phytoplankton absorption at 440 nm is modeled as [*Bricaud et al*., 1995]

$$a_{ph}(440) = 0.05[CHL]^{0.626} \tag{4}$$

The phytoplankton absorption spectrum, $a_{ph}(\lambda)$, is simulated as

$$a_{ph}(\lambda) = a_{ph}(440) \cdot a_{ph}^{+}(\lambda) \tag{5}$$

where $a_{ph}^{+}$ is the 440 nm normalized absorption coefficient of phytoplankton and is randomly chosen from the IOCCG data set [*IOCCG*, 2006]. According to *Bricaud et al*. [2010], the spectral shape of $a_{ph}^{+}$ is approximately symmetrical about 440 nm within the spectral range from 360 to 520 nm. So the spectral values of $a_{ph}^{+}$ at UV wavelengths (360, 370, 380, and 390 nm) are assumed equal to $a_{ph}^{+}(520)$, $a_{ph}^{+}(510)$, $a_{ph}^{+}(500)$, and $a_{ph}^{+}(490)$, respectively. The ratio of $a_{cdom}(440)/a_{ph}(440)$ is assumed to be 0.5 and 1, respectively, for each of the two types of waters. Such assignments of ratios were approximated from the global distribution of CDOM [*Siegel et al*., 2002]. The absorption spectrum of CDOM, $a_{cdom}(\lambda)$, is derived from equation (2), with the spectral slope $S_{cdom}$ varying from 0.008 to 0.024 $nm^{-1}$ with a step of 0.002 $nm^{-1}$, a range covering the reported results for $S_{cdom}$ [*Babin et al*., 2003; *Binding et al*., 2008]. We assigned a constant 0.1 to the ratio of $a_{det}(440)/a_{cdom}(440)$, considering that the detrital materials usually represent a minor component of the total absorption in upper ocean waters [*Bricaud et al*., 2010; *Siegel et al*., 2002]. To further simplify, the spectral slope of $a_{det}(\lambda)$, $S_{det}$, was assumed to vary sequentially from 0.004 to 0.020 $nm^{-1}$ at a step of 0.002 $nm^{-1}$. It is noted that, because of the predominance of $a_{cdom}(440)$ over $a_{cdm}(440)$ and because the typical spectral slope parameters for particulate detrital absorption are noticeably smaller than those found for CDOM [*Nelson and Siegel*, 2002], the spectral absorption $a_{cdm}(\lambda)$ is dominated by $a_{cdom}(\lambda)$ and the assumed covariation between $a_{det}(440)$ and $a_{cdom}(440)$ does not impact the subsequent conclusions. It should be noted that in nearshore ocean waters, $a_{det}(440)$ is significant in magnitude and could be larger than $a_{cdom}(440)$ [*Pan et al*., 2008]. The particle backscattering coefficient is modeled as a power function of chlorophyll-a concentration [*Huot et al*., 2008]

$$b_{bp} = \alpha \cdot [CHL]^{\beta} \tag{6}$$

with two coefficients $\alpha$ and $\beta$ being modeled as [*Huot et al*., 2008]

$$\begin{aligned} \alpha &= 2.267\times10^{-3} - 5.058\times10^{-6}(\lambda - 550) \\ \beta &= 0.565 + 0.000486(\lambda - 550) \end{aligned} \tag{7}$$

A total of 54 combinations of inherent optical properties were used for oceanic waters (2 [CHL] levels × 9 levels of $S_{cdom}$ and $S_{det}$ × 3 levels of $a_{cdom}(440)$ = 54 combinations).

The light field for the total of 54 combinations of IOPs were further simulated with Hydrolight 5 [*Mobley and Sundman*, 2008]. For every simulation, the wind speed was set to 5 m $s^{-1}$, with the solar zenith angle at 30°. The absorption coefficient of pure seawater $a_w$ between 360 to 550 nm is adopted from *Lee et al*. [2015]. The $a_w$ at wavelengths longer than 550 nm follows the measurements of *Pope and Fry* [1997]. The backscattering coefficient of pure seawater, $b_{bw}$, takes the results of *Morel* [1974]. A constant backscattering ratio of 0.018 for particulate components is assumed [*Mobley*, 1994]; this assumption is sufficient for our study, although the backscattering ratios can be highly variable in natural waters thus affect the magnitude of $R_{rs}$ [*Tzortziou et al*., 2006].

Figures 2a and 2b illustrate the modeled $R_{rs}$ and IOPs for water with [CHL] = 0.07 mg $m^{-3}$. For such waters, $a_{cdom}(440)$ is sometimes found smaller than phytoplankton absorption in the upper oceans [*Bricaud et al*., 2010; *Morel and Gentili*, 2010]. Because $a_{det}(\lambda)$ is much smaller than $a_{cdom}(\lambda)$, the spectral slope $S_{cdm}$ is predominated by that of $a_{cdom}(\lambda)$, with values approximately the same as those of $S_{cdom}$. Although $S_{cdm}$ varies widely in the simulations, a weak variation is found in the modeled $R_{rs}$ spectra in the visible spectral region. The impact of varying $S_{cdm}$, however, is considerable in the blue and UV spectral regions and, as expected, the impact increases with decreasing wavelengths. This is consistent with the field measured $R_{rs}$ (Figure 1).

The simulated $R_{rs}$ and IOPs for ocean waters with higher chlorophyll-a (0.15 mg $m^{-3}$) are shown in Figures 2c and 2d, respectively. In these waters, the ratio of $a_{cdom}(440)$ to $a_{ph}(440)$ was assumed to be 1, while the $S_{cdom}$ values also varied from 0.008 to 0.024 $nm^{-1}$. In analogy to the oceans with lower [CHL], the $R_{rs}$ spectra in the UV bands vary over a wide range. On the other hand, the $R_{rs}$ spectra at most of the visible wavelengths are relatively hard to discern from each other. These unique spectral signatures presented in Figure 2c are also very similar to the $R_{rs}$ spectra shown in Figure 1.

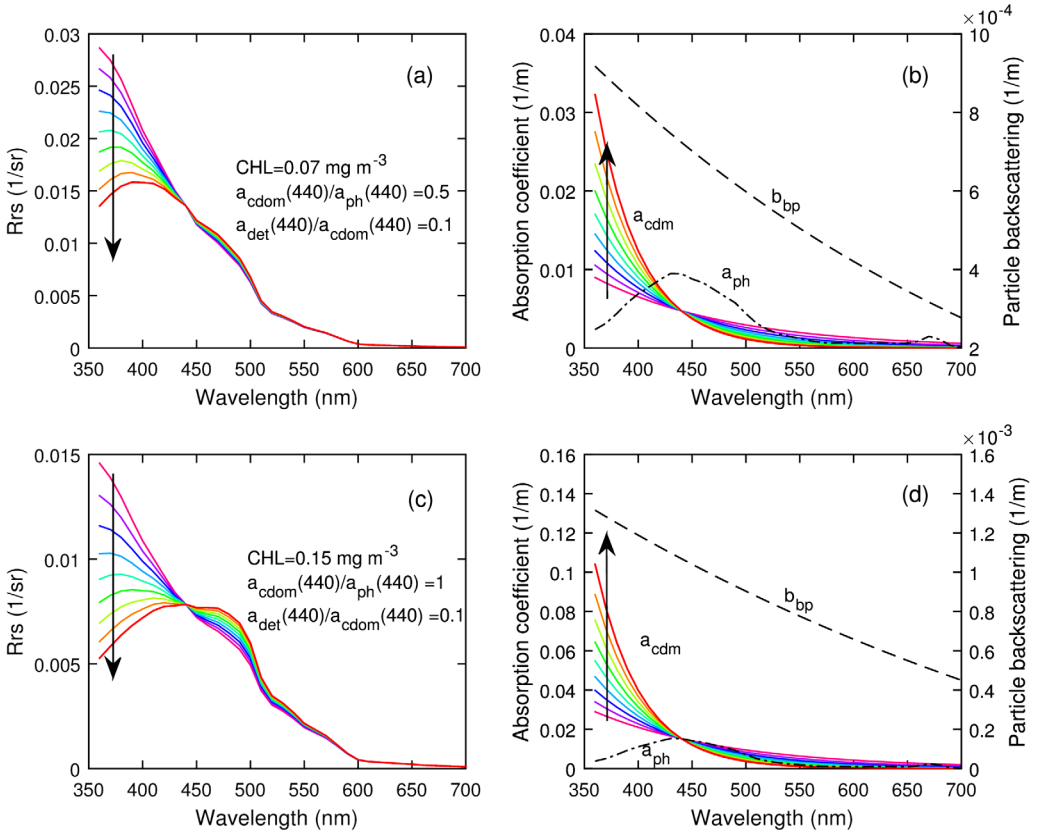


**Figure 2.** Variation of $R_{rs}$ spectra shapes with different spectral slopes of CDOM in two oceanic waters. The CDOM absorption spectra are denoted in solid colored lines, phytoplankton absorption in black dash-dot line, and particle backscattering in black dash line. The absorption ratios are given in the figure. The black arrows denote the trend of increasing spectral slope from *Scdm* $\approx$ 0.008 nm$^{-1}$ to 0.024 nm$^{-1}$.

In the above simulations, the spectral slopes of CDOM and detritus were varied, but the relative ratios of CDOM and detrital material absorption to chlorophyll a absorption at 440 nm were kept constant. However, the relative contributions of different water constituents are highly variable in natural waters. To account for this complexity, three cases of waters were further simulated, where the phytoplankton absorption was kept the same (with [CHL] = 0.07 mg m$^{-3}$) while the ratio of $a_{cdom}(440)/a_{ph}(440)$ increased from 0.5, to 1 to 2, with a constant spectral slope $S_{cdom}$ = 0.016 nm$^{-1}$. Similarly, the ratio $a_{det}(440)/a_{cdom}(440)$ was kept constant at 0.1. Consequently the CDM had a spectral slope $S_{cdm} \approx$ 0.014 nm$^{-1}$. As shown in Figure 3, the magnitudes of the $R_{rs}$ spectra are considerably lower with the increase of $a_{cdom}(440)/a_{ph}(440)$ ratios. This is expected, because the increased $a_{cdm}(440)/a_{ph}(440)$ ratios lead to increased total absorption coefficient for a given value of $a_{ph}(440)$, and ultimately to decreased $R_{rs}$ (equation (1)). Also, the difference in the $R_{rs}$ spectra becomes larger with decreasing wavelengths because of the exponential spectral shape in $a_{cdm}$. When $a_{cdm}(440)/a_{ph}(440)$ increased from ~0.5 to 1, for example, the relative difference of spectral $R_{rs}$ increases significantly from red bands to UV bands, with $\Delta|R_{rs}(670)| \approx 0$ sr$^{-1}$, $\Delta|R_{rs}(550)| = 0.00004$ sr$^{-1}$, $\Delta|R_{rs}(440)| = 0.0027$ sr$^{-1}$, and $\Delta|R_{rs}(380)| = 0.0073$ sr$^{-1}$. The spectral variation of $\Delta|R_{rs}(\lambda)|$ in the UV-visible domain found in these cases does not mimic that from field measurements shown in Figure 1 and the simulations in Figure 2.

The impact of varying $b_{bp}(\lambda)$ values on the $R_{rs}$ spectrum is not expected to show a strong spectral dependence. Thus the observed difference in $R_{rs}$(UV) could not be interpreted as the influence of different $b_{bp}(\lambda)$ values.

To sum up, the spectral slope of CDOM and detritus is a dominant factor forming the unique contrast of $R_{rs}$ spectra observed in Figure 1. Other optical parameters including $a_{cdm}(440)$, $b_{bp}(\lambda)$ as well as $a_{ph}(\lambda)$ also play a role but likely to be secondary for such spectral patterns. As a result, including UV wavebands in the ocean color inversion will lead to more accurate retrieval of $S_{cdm}$.

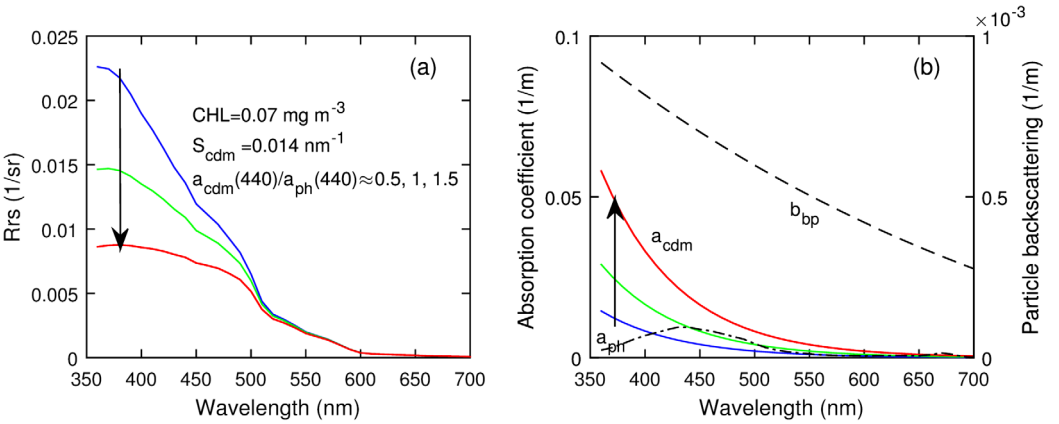


**Figure 3.** Variation of $R_{rs}$ spectra shapes with the amplitude of CDOM and detrital material absorption $a_{cdm}(440)$. The black arrows denote the trend of increasing $a_{cdm}(440)$, with the ratio of $a_{cdm}(440)/a_{ph}(440)$ increasing from roughly 0.5, to 1, to 2.

## 4. Assessment of the Spectral Slope of CDM Absorption Coefficient From UV-Visible Ocean Color

Since $R_{rs}(\lambda)$ in the UV wavelengths is mostly sensitive to the variation in $S_{cdm}$, addition of UV wavelengths to the visible ocean color is expected to improve the retrieval of $S_{cdm}$. In this section, we examine the feasibility of such retrievals and assess the degree of improvement in the estimated $S_{cdm}$ after including UV wavelengths (sections 4.3). The impact of including UV bands in the $R_{rs}$ spectra on the retrieval of $a_{ph}(\lambda)$ and $a_{cdm}(\lambda)$ is also discussed (section 4.4). Ideally we should seek an analytical retrieval of both $a_{det}$ and $a_{cdom}$ spectra, but initial tests (not shown here) resulted in nonunique solution via spectral optimization, therefore we still focus on the retrieval of $a_{cdm}$ as in traditional practices. This way it also reduces the number of variables to be derived from an $R_{rs}$ spectrum.

### 4.1. Evaluation Data

Hyperspectral data of the inherent optical properties spanning the UV and visible wavelengths (10 nm band intervals) are synthesized. We choose the first 150 sets of inherent optical properties from the IOCCG data [*IOCCG*, 2006] as the basis for this assessment, which represent a large variety of blue oceanic waters. These data were originally synthesized to simulate waters with [CHL] $< \sim$0.2 mg m$^{-3}$, a range of chlorophyll-a concentrations representing a majority of global oceans. It is emphasized that the spectral shapes of phytoplankton absorption spectra in the IOCCG database were composed from extensive measurements of *Bricaud et al.* [1995], *Bricaud et al.* [1998], and *Carder et al.* [1999] to represent the natural variation of $a_{ph}$ spectra. The IOCCG data were synthesized in the 400–700 nm range (with 10 nm spectral resolution), which were expanded to the UV wavelengths in this study. Specifically, the backscattering coefficient of particles is extrapolated to 360 nm following the power-law function (equation (3)) [*Gordon and Morel*, 1983]. The particle backscattering ratios of 0.01 and 0.018 are assumed for phytoplankton and detrital matters, respectively. The corresponding Fournier-Forand scattering phase functions are selected by Hydrolight 5 [*Mobley and Sundman*, 2008] based on the backscattering ratios. And similarly, the CDOM and detritus absorption coefficients, respectively, are extrapolated to UV domain following equation (2), with their original spectral slopes. The phytoplankton absorption spectrum at wavelength 360 is assumed equal to $a_{ph}(520)$, and then $a_{ph}(370)$, $a_{ph}(380)$, and $a_{ph}(390)$ are linearly interpolated between $a_{ph}(360)$ and $a_{ph}(440)$. The absorption coefficient of pure seawater between 360 and 550 nm is adopted from *Lee et al.* [2015]; otherwise, the default values of pure seawater properties are used in the Hydrolight simulations. Raman scattering or fluorescence is excluded following the original data simulation. The sky is assumed to be clear with a solar zenith angle at 30°, and a wind speed of 5 m s$^{-1}$. Figure 4a shows the simulated remote sensing reflectance from 360 to 700 nm, while Figures 4b–4d plot the inherent optical properties. The spectral slope for the colored dissolved and detrital matters varies approximately from 0.01 to 0.02 nm$^{-1}$.

Unlike the Hydrolight-simulated $R_{rs}$ data, which in general are considered "error-free," the remote sensing reflectance obtained from a satellite sensor is subject to large noises ($\varepsilon$) due to imperfect atmospheric correction [*Antoine et al.*, 2008; *Gordon*, 1997; *Hu et al.*, 2013]. This noise will pose challenges to subsequent

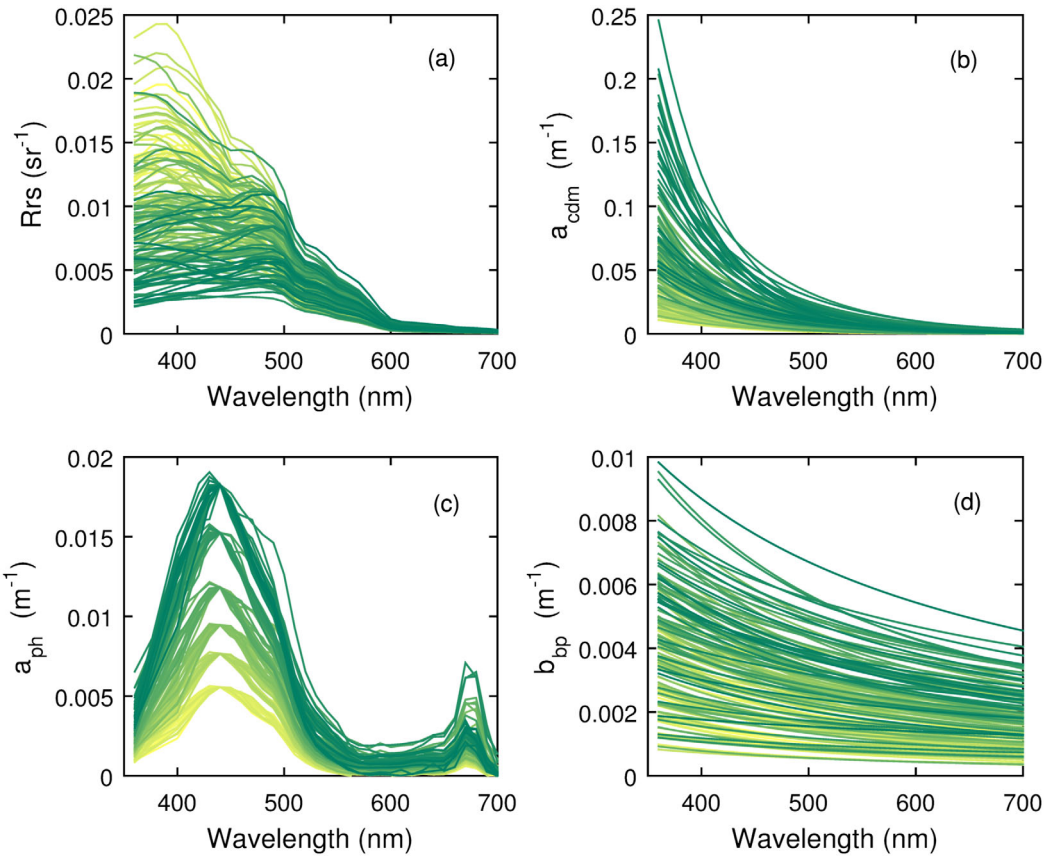


**Figure 4.** Evaluation data developed from IOCCG's first 150 data sets.

efforts of ocean color inversions [*Wei and Lee*, 2015]. To assess the potential impacts of $\varepsilon$ on the retrieval of $S_{cdm}$, we designed and implemented the following analyses. First, the remotely measured ocean color $R_{rs}^{OC}$ was composed of two contributors: the "true" $R_{rs}$ spectrum and a spectrally dependent noise term $\varepsilon$ from the atmospheric correction procedure

$$R_{rs}^{OC}(\lambda) = R_{rs}(\lambda) + \varepsilon(\lambda) \tag{8}$$

*Hu et al.* [2013] quantified the errors of SeaWiFS and MODIS Aqua ocean color data in the ocean gyres and found that $\varepsilon(\lambda)$ is spectrally covariant, increasing from the red wavelength at 670 nm toward the blue wavelength at 410 nm. To simulate such errors, we first interpolated the tabulated errors of both sensors of *Hu et al.* [2013] to seven wavelengths at 410, 440, 490, 510, 530, 550, and 670 nm, and then all these new interpolated errors were grouped together according to the wavelength. The average errors for every wavelength were determined and further fitted to the following linear model, $\varepsilon(\lambda) = -1.898 \times 10^{-6}(\lambda - 670) + \varepsilon(670)$, with the average value of $\varepsilon(670)$ equal to $6.559 \times 10^{-5}$ sr$^{-1}$. With this model, the spectrum of the noise function between 360 and 700 nm was determined from $\varepsilon(670)$, which is predicted by random numbers of normal distribution with a mean value equal to $6.559 \times 10^{-5}$ sr$^{-1}$ and standard deviation of $2.463 \times 10^{-5}$ sr$^{-1}$. Such simulated spectral errors $\varepsilon(\lambda)$ were then added to the Hydrolight-simulated $R_{rs}$ spectra discussed above.

Both the "error-free" and "error-disturbed" evaluation data are examined in the following for the effects of including UV wavebands in the ocean color inversions.

### 4.2. Optimization Inversion Scheme

The hyperspectral optimization process exemplar (HOPE), originally developed for remote sensing of shallow waters [*Lee et al.*, 1999], was applied to assess a semianalytical retrieval of $S_{cdm}$ from remote sensing

reflectance. Because the focus is on deep waters, the terms associated with a shallow bottom in HOPE are excluded. Second, the model of phytoplankton spectral absorption is now extended to the UV domain

$$a_{ph}(\lambda)=\left[a_0+a_1\ln\left(a_{ph}(440)\right)\right]\cdot a_{ph}(440) \tag{9}$$

where the model coefficients $a_0$ and $a_1$ in the UV and visible domain are obtained by fitting the model function to the synthetic evaluation data. After the optical models for IOPs, there are five variables ($a_{ph}(440)$, $a_{cdm}(440)$, $b_{bp}(440)$, $\eta$, and $S_{cdm}$) for a given $R_{rs}$ spectrum. To implement HOPE, five initial values for $a_{ph}(440)$, $a_{cdm}(440)$, $b_{bp}(440)$, $\eta$, and $S_{cdm}$ are provided as the following: $a_{ph}(440) = 0.05\times[R_{rs}(440)/R_{rs}(550)]^{-1.62}$, $a_{cdm}(440) = 0.5 \times a_{ph}(440)$, $b_{bp}(440) = 30 \times a_w(670) \times R_{rs}(670)$, $S_{cdm} = 0.015$, and $\eta = 0.6$. The spectral values for $a_{ph}(\lambda)$, $a_{cdm}(\lambda)$ and $b_{bp}(\lambda)$ are then derived following equations (9), (2), and (3), respectively. With the estimated $a_{ph}(\lambda)$, $a_{cdm}(\lambda)$, $b_{bp}(\lambda)$, the remote sensing reflectance just below the water surface ($r_{rs}$, $sr^{-1}$) can be modeled following *Lee et al.* [2004], where the molecular and particle scattering effects are accounted explicitly,

$$r_{rs}(\lambda)=G_w\frac{b_{bw}(\lambda)}{a(\lambda)+b_b(\lambda)}+G_p(\lambda)\frac{b_{bp}(\lambda)}{a(\lambda)+b_b(\lambda)} \tag{10}$$

where $G_w$ and $G_p(\lambda)$ are two model coefficients, with $G_w = 0.113\ sr^{-1}$ and $G_p(\lambda)$ further modeled as

$$G_p(\lambda)=G_0\left[1-G_1\exp\left(-G_2\frac{b_{bp}(\lambda)}{a(\lambda)+b_b(\lambda)}\right)\right] \tag{11}$$

where three coefficients ($G_0$, $G_1$, $G_2$) are modeled as constants, with $G_0 = 0.197\ sr^{-1}$, $G_1 = 0.636$, and $G_2 = 2.552$ [*Lee et al.*, 2004]. The remote sensing reflectance just above the water is then derived from the following model [*Lee et al.*, 2002]

$$R_{rs}=\frac{0.52r_{rs}}{1-1.7r_{rs}} \tag{12}$$

Such estimated $R_{rs}$ is then compared with the input $R_{rs}$ spectrum through the following cost function,

$$Err=\frac{\sqrt{\frac{1}{N}\sum_{i=1}^{N}\left({R_{rs}}^{est}(\lambda_i)-{R_{rs}}^{true}(\lambda_i)\right)^2}}{\frac{1}{N}\sum_{i=1}^{N}{R_{rs}}^{true}(\lambda_i)} \tag{13}$$

where $R_{rs}^{est}$ and $R_{rs}^{true}$ refer to the estimated and input remote sensing reflectance, respectively. In equation (13), all the wavelengths of valid $R_{rs}$ (360–700 nm or 410–700 nm) are used.

The following constraints are applied to the five variables: $a_{ph}(440)$, $a_{cdm}(440)$, $S_{cdm}$, $b_{bp}(440)$, and $\eta$, with $0.002<a_{ph}(440)<0.2\ m^{-1}$, $0.002<a_{cdm}(440)<0.045\ m^{-1}$, and $0.003<S_{cdm}<0.028\ nm^{-1}$, $0.0006<b_{bp}(440)<0.008\ m^{-1}$, and $0.55<\eta<2.2$, respectively, which are determined from the synthetic data set itself. The constrained nonlinear optimization minimized the objective function of equation (13) using the interior-point algorithm [*Byrd et al.*, 1999]. The maximum iteration was set to 10,000, and the tolerance was $1 \times 10^{-20}$.

To evaluate the model performance, we adopted the following error metrics. The root-mean square error (RMSE) is derived as

$$RMSE=\sqrt{\frac{1}{N}\sum_{i=1}^{N}\left[\left(S_i^{est}\right)^2-\left(S_i^{true}\right)^2\right]} \tag{14}$$

with $S_i^{est}$ and $S_i^{true}$ the model estimated quantity and known quantity, respectively. The mean absolute percentage error ($\delta$) is defined as

$$\delta=\frac{1}{N}\sum_{i=1}^{N}\left|\frac{S_i^{est}-S_i^0}{S_i^0}\right|\times 100\% \tag{15}$$

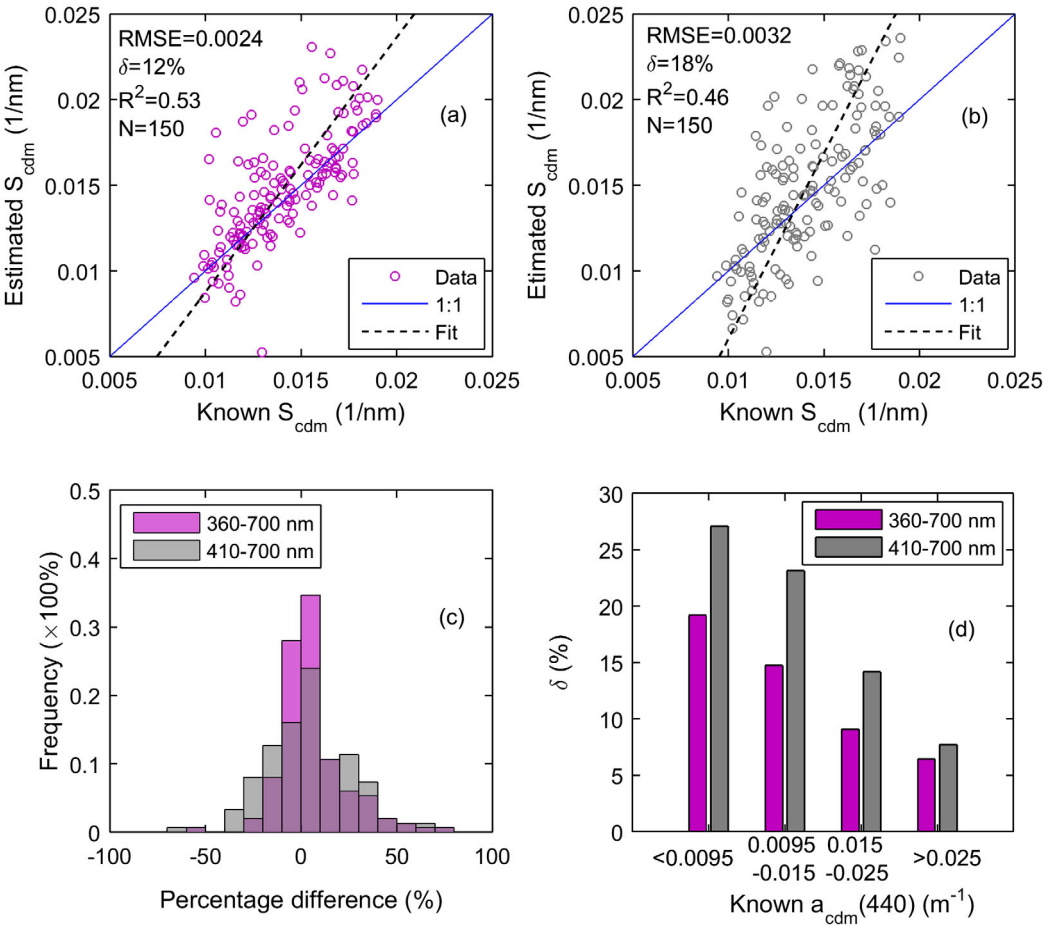


**Figure 5.** Model-retrieved spectral slopes of CDM from "error-free" remote sensing reflectance. (a) Hyperspectral reflectance at all available wavelengths from 360 to 700 nm is used; (b) Hyperspectral reflectance between 410 nm to 700 nm is used; (c) Frequency distribution of %diff for the estimated $S_{cdm}$ from $R_{rs}$(UV + Vis) and $R_{rs}$(Vis); (d) Comparison of the absolute percentage errors ($\delta$) for $S_{cdm}$ retrieved in four subgroups of waters. The numbers of observations available for the comparisons in subplot (d) are 37 (for $a_{cdm}(440)<0.0095$ m$^{-1}$), 30 (for $0.0095< a_{cdm}(440)<0.015$ m$^{-1}$), 47 (for $0.015< a_{cdm}(440)<0.025$ m$^{-1}$), and 36 (for $a_{cdm}(440)>0.025$ m$^{-1}$).

### 4.3. Effects of Including UV Bands on $S_{cdm}$ Retrievals

The "error-free" evaluation data are first used for the assessment. Figure 5 compares two sets of $S_{cdm}$ retrievals: one using $R_{rs}$ spectra from 360 to 700 nm ($R_{rs}$(UV+Vis) hereafter) and another one using the visible ocean color from 410 to 700 nm ($R_{rs}$(Vis) hereafter). From $R_{rs}$(UV+Vis), good agreement is observed between the model retrieved and known $S_{cdm}$ with an RMSE value around 0.0024 nm$^{-1}$ and $\delta$ around 12% (Figure 5a). The coefficient of determination ($R^2$) between the two sets of $S_{cdm}$ is 0.53. Note that the $R^2$ value is very sensitive to the data range used for such evaluations, and the $S_{cdm}$ values evaluated here is quite narrow (roughly between 0.01 and 0.02 nm$^{-1}$). The type-II linear fitting also indicates that the estimated $S_{cdm}$ represents the known $S_{cdm}$ very well except for a few outliers (Figure 5a and Table 2).

The $S_{cdm}$ retrievals from $R_{rs}$(Vis) are compared with known values in Figure 5b. It is found that the $S_{cdm}$ derived from $R_{rs}$(Vis) is subject to larger errors and uncertainties than those derived from $R_{rs}$(UV+Vis). Specifically, the RMSE value has increased to 0.0032 nm$^{-1}$, with $\delta$ increased to 18%, and $R^2$ decreased to 0.46. These increases in the model errors highlight the value of including UV bands in the $R_{rs}$ inversions, as this is the spectral range that is more sensitive to the change of $S_{cdm}$.

We further assessed the relative percentage error, $\%\text{diff} = (S^{est} - S^{true})/S^{true} \times 100\%$, for the two sets of $S_{cdm}$ and compared their frequency distributions in Figure 5c. When $S_{cdm}$ was derived from $R_{rs}$(UV+Vis) in the inversion process, the %diff is distributed in a much narrower range of $\pm$10% for more than 60% of observations and more tightly centered around zero. Clearly, the uncertainty in HOPE derived $S_{cdm}$ is significantly reduced by including ocean color information in the UV bands.

**Table 2.** Error Statistics for the Estimated $S_{cdm}$ Using the Simulated "Error-Free" $R_{rs}$

| Spectral domain (nm) | RMSE ($nm^{-1}$) | $\delta$ | $R^2$ | Slope of Linear Fit | Intercept of Linear Fit |
|---|---|---|---|---|---|
| 360–700 | 0.0024 | 12% | 0.53 | 0.672 | 0.0041 |
| 360,380,410–700 | 0.0022 | 11% | 0.58 | 0.706 | 0.0037 |
| 360, 410–700 | 0.0027 | 13% | 0.47 | 0.602 | 0.0051 |
| 380, 410–700 | 0.0031 | 14% | 0.38 | 0.491 | 0.0068 |
| 410–700 | 0.0034 | 18% | 0.46 | 0.461 | 0.0072 |

The IOCCG data are further divided into four subgroups of waters, each of which is characterized by distinctive $a_{cdm}(440)$. Specifically, these subgroups are defined by the following ranges of $a_{cdm}(440)$ values: $a_{cdm}(440)$ $<0.0095$ $m^{-1}$, $0.0095< a_{cdm}(440) <0.015$ $m^{-1}$, $0.015< a_{cdm}(440) <0.025$ $m^{-1}$, and $a_{cdm}(440)$ $>0.025$ $m^{-1}$. Our results show that the $S_{cdm}$ retrievals from $R_{rs}$(UV+Vis) are also superior to those from $R_{rs}$(Vis) for such specific cases (Figure 5d). In particular, the effect on the accuracy of $S_{cdm}$ retrievals is more evident from $R_{rs}$(UV+Vis) for waters with relatively lower $a_{cdm}(440)$.

When the input $R_{rs}$ spectrum contains errors or is "error-disturbed," the ocean color inverted $S_{cdm}$ is found subject to relatively larger errors (see Figure 6 and Table 3). Despite the degradations in the retrieval accuracy, the advantages of including UV bands in the ocean color inversion of $S_{cdm}$ are still obvious. Comparing Figures 6a and 6b, the $S_{cdm}$ estimated from $R_{rs}$(UV+Vis) are more accurate than those without using UV bands. Out of the total of 150 points, about 65% of the retrievals are found with a relative error within $\pm$20% when the UV wavelengths are used (Figure 6c). For the subgroups of waters with distinctive

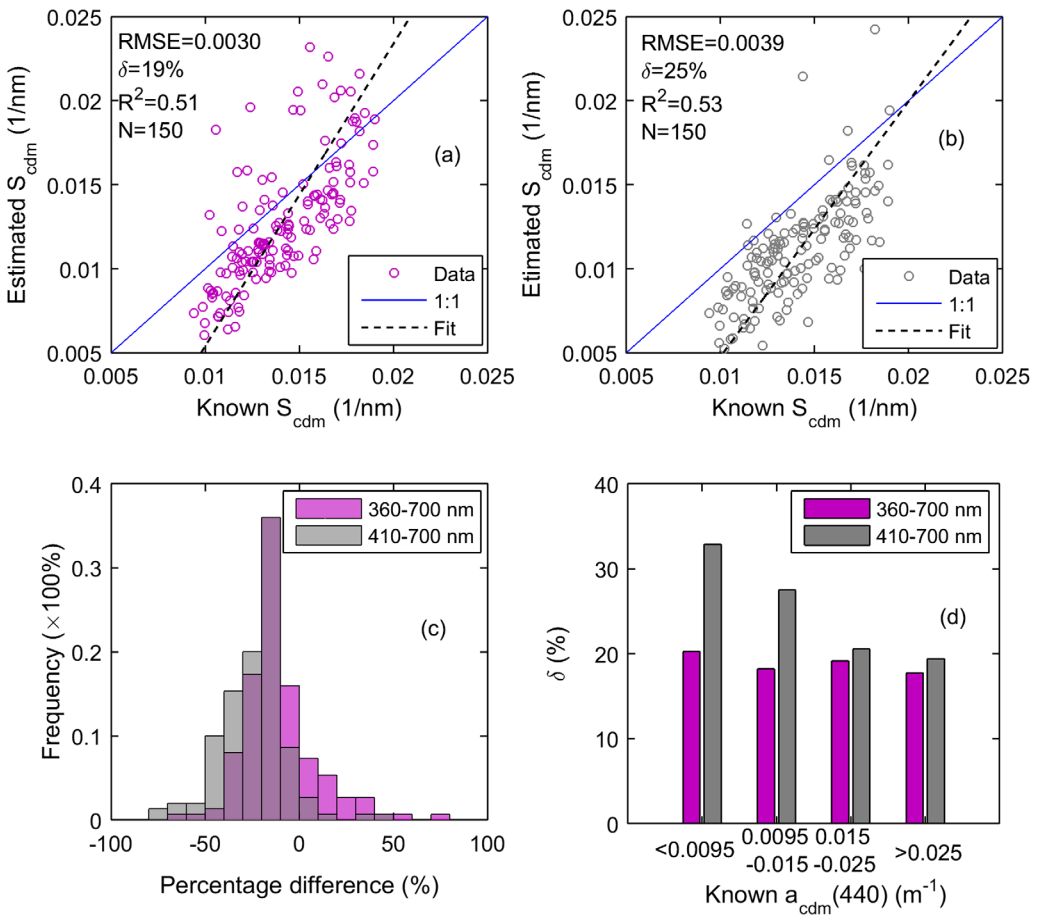


**Figure 6.** Model-retrieved spectral slopes of CDM from "error-disturbed" remote sensing reflectance. (a) Hyperspectral reflectance at all available wavelengths from 360 to 700 nm is used; (b) Hyperspectral reflectance between 410 to 700 nm is used; (c) Frequency distribution of %diff for the estimated $S_{cdm}$ from $R_{rs}$(UV + Vis) and $R_{rs}$(Vis); (d) Comparison of the absolute percentage errors ($\delta$) for $S_{cdm}$ retrieved in four subgrouped waters (same groups as Figure 5d).

**Table 3.** Error Statistics of the Estimated $S_{cdm}$ Using the "Error-Disturbed" $R_{rs}$

| Spectral domain (nm) | RMSE ($nm^{-1}$) | $\delta$ | $R^2$ | Slope of Linear Fit | Intercept of Linear Fit |
|---|---|---|---|---|---|
| 360–700 | 0.0031 | 19% | 0.51 | 0.556 | 0.0070 |
| 360,380,410–700 | 0.0031 | 20% | 0.54 | 0.568 | 0.0070 |
| 360, 410–700 | 0.0036 | 22% | 0.41 | 0.454 | 0.0084 |
| 380, 410–700 | 0.0038 | 23% | 0.42 | 0.476 | 0.0084 |
| 410–700 | 0.0039 | 25% | 0.53 | 0.658 | 0.0069 |

$a_{cdm}$(440) values, the accuracy in the retrieved $S_{cdm}$ is consistently better when derived from $R_{rs}$(UV+Vis) (Figure 6d). The best performance is found in waters with relatively lower $a_{cdm}$(440) values.

The above analyses are based on the hyperspectral $R_{rs}$ data with even spectral spacing of 10 nm. We further investigated whether the number of UV wavelengths chosen for the model runs will impact the model estimations. The HOPE optimization runs were implemented using $R_{rs}$ in the visible (410–700 nm) and a varying number of UV bands; in our case, either one or two or all UV wavelengths were selected from $R_{rs}$(360–400 nm) and added to the visible $R_{rs}$ spectra. The error statistics for the estimated $S_{cdm}$ are summarized in Table 2 for "error-free" $R_{rs}$ data and in Table 3 for the "error-disturbed" $R_{rs}$ data. Our results indicate that simply including two UV wavelengths at 360 and 380 nm with $R_{rs}$(Vis) in the inversions will significantly increase the accuracy of $S_{cdm}$, with reduced RMSE and $\delta$, and enhanced $R^2$. Furthermore, including both UV wavelengths (360 and 380 nm) will lead to more accurate retrievals of $S_{cdm}$ than merely using one of the two. Besides, the uncertainty of the estimated $S_{cdm}$, in terms of the %diff, is also significantly reduced when the two or more UV wavelengths are included (not shown for brevity).

### 4.4. Effects of Including UV Bands on $a_{ph}(\lambda)$ and $a_{cdm}(\lambda)$ Retrievals

Besides the spectral slope of CDM absorption coefficient, the phytoplankton and CDM absorption coefficients at 440 nm are also simultaneously retrieved from the HOPE inversion procedures. We first compared the model estimations from the "error-free" $R_{rs}$ data and summarized them in Table 4. It is found that the overall improvement in $a_{ph}$(440) retrieval is rather limited, and the retrieved $a_{cdm}$(440) shows basically no improvement. This result reflects the observation that the changes of $R_{rs}$ in the UV are mainly a change of $S_{cdm}$ rather the change of $a_{ph}$(440) or $a_{cdm}$(440) values. When propagating the estimated $a_{cdm}$(440) to other wavelengths with the retrieved $S_{cdm}$ from equation (2), some limited improvements can be found in the

**Table 4.** Error Statistics for the Estimated Optical Properties Using the UV-Visible Remote Sensing Reflectance (360–700 nm)[a]

| Parameters | RMSE ($nm^{-1}$) | $\delta$ | $R^2$ | Slope of Linear Fit | Intercept of Linear Fit |
|---|---|---|---|---|---|
| $S_{cdm}$ | 2.38E-03 | 12% | 0.53 | 0.672 | 4.10E-03 |
| | (3.52E-03) | (18%) | (0.46) | (0.461) | (7.22E-03) |
| $a_{ph}$(440) | 2.01E-03 | 12% | 0.81 | 0.967 | 5.44E-04 |
| | (2.11E-03) | (16%) | (0.80) | (0.925) | (9.74E-04) |
| $a_{cdm}$(440) | 4.44E-03 | 20% | 0.90 | 1.058 | 2.40E-04 |
| | (4.40E-03) | (19%) | (0.90) | (1.059) | (3.10E-04) |
| $b_{bp}$(440) | 4.42E-04 | 13% | 0.92 | 1.002 | 1.14E-04 |
| | (3.64E-04) | (9%) | (0.95) | (1.031) | (3.97E-05) |
| $a_{cdm}$(360) | 6.93E-03 | 9% | 0.98 | 1.063 | −9.59E-04 |
| | (7.29E-03) | (9%) | (0.98) | (1.062) | (−8.11E-04) |
| $a_{cdm}$(380) | 6.36E-03 | 12% | 0.97 | 1.067 | −5.45E-04 |
| | (6.17E-03) | (9%) | (0.97) | (1.069) | (−4.25E-04) |
| $a_{cdm}$(490) | 3.03E-03 | 26% | 0.82 | 1.021 | 4.92E-04 |
| | (3.09E-03) | (29%) | (0.81) | (1.016) | (4.95E-04) |
| $a_{cdm}$(530) | 2.19E-03 | 31% | 0.76 | 0.976 | 5.15E-04 |
| | (2.27E-03) | (37%) | (0.74) | (0.964) | (4.84E-04) |
| $a_{ph}$(360) | 1.52E-03 | 44% | 0.38 | 0.499 | 9.73E-04 |
| | (1.63E-03) | (52%) | (0.35) | (0.456) | (1.09E-03) |
| $a_{ph}$(380) | 1.58E-03 | 24% | 0.63 | 0.822 | 8.34E-04 |
| | (1.67E-03) | (28%) | (0.62) | (0.777) | (1.04E-03) |
| $a_{ph}$(490) | 1.56E-03 | 14% | 0.67 | 1.002 | 8.90E-05 |
| | (1.64E-03) | (20%) | (0.65) | (0.955) | (3.85E-04) |
| $a_{ph}$(530) | 8.21E-04 | 36% | 0.31 | 1.409 | −7.01E-04 |
| | (8.64E-04) | (44%) | (0.27) | (1.336) | (−5.83E-04) |

[a]The values given in the parentheses refer to the error statistics when limiting the spectral $R_{rs}$ to the visible bands (410–700 nm) only.

**Table 5.** Error Statistics for the Estimated Optical Properties Using the "Error-Disturbed" UV-Visible Remote Sensing Reflectance (360–700 nm)[a]

| Parameters | RMSE ($nm^{-1}$) | $\delta$ | $R^2$ | Slope of Linear Fit | Intercept of Linear Fit |
|---|---|---|---|---|---|
| $S_{cdm}$ | 3.01E-03 | 19% | 0.51 | 0.556 | 7.00E-03 |
| | (3.91E-03) | (25%) | (0.53) | (0.658) | (6.87E-03) |
| $a_{ph}(440)$ | 3.28E-03 | 21% | 0.63 | 1.117 | 7.40E-04 |
| | (3.19E-03) | (22%) | (0.76) | (0.991) | (2.38E-03) |
| $a_{cdm}(440)$ | 4.66E-03 | 19% | 0.88 | 0.996 | 1.32E-04 |
| | (4.33E-03) | (17%) | (0.90) | (1.069) | (−2.22E-03) |
| $b_{bp}(440)$ | 4.30E-04 | 14% | 0.933 | 1.025 | −2.51E-04 |
| | (4.36E-04) | (16%) | (0.946) | (1.065) | (−4.73E-04) |
| $a_{cdm}(360)$ | 1.50E-02 | 16% | 0.98 | 1.269 | −4.23E-03 |
| | (1.66E-02) | (18%) | (0.97) | (1.289) | (−3.48E-03) |
| $a_{cdm}(380)$ | 9.92E-03 | 14% | 0.96 | 1.119 | −2.35E-03 |
| | (1.05E-02) | (14%) | (0.96) | (1.231) | (−3.23E-03) |
| $a_{cdm}(490)$ | 3.78E-03 | 30% | 0.80 | 0.838 | 5.88E-04 |
| | (3.78E-03) | (35%) | (0.82) | (0.931) | (−1.31E-03) |
| $a_{cdm}(530)$ | 3.20E-03 | 42% | 0.74 | 0.722 | 6.05E-04 |
| | (3.33E-03) | (56%) | (0.75) | (0.813) | (−7.10E-04) |
| $a_{ph}(360)$ | 1.34E-03 | 38% | 0.29 | 0.588 | 1.09E-03 |
| | (1.38E-03) | (41%) | (0.38) | (0.533) | (1.30E-03) |
| $a_{ph}(380)$ | 1.95E-03 | 30% | 0.49 | 0.976 | 9.76E-04 |
| | (1.97E-03) | (30%) | (0.59) | (0.856) | (1.67E-03) |
| $a_{ph}(490)$ | 2.14E-03 | 20% | 0.52 | 1.171 | 7.90E-05 |
| | (2.04E-03) | (21%) | (0.67) | (1.024) | (1.20E-04) |
| $a_{ph}(530)$ | 9.11E-04 | 34% | 0.23 | 1.888 | −1.01E-03 |
| | (9.05E-04) | (34%) | (0.30) | (1.482) | (−2.98E-04) |

[a]The values given in the parentheses refer to the error statistics when limiting the spectral $R_{rs}$ to the visible bands (410–700 nm) only.

inverted results at longer wavelengths from $R_{rs}$(UV+Vis). The spectral phytoplankton absorption $a_{ph}(\lambda)$ is further derived from equation (9) based on the inverted $a_{ph}(440)$. It is found that, at least to this data set, the phytoplankton absorption coefficients at 360, 380, 490, and 530 nm are improved to a very limited degree considering both RMSE and $\delta$.

When the $R_{rs}$ spectra are "error disturbed," basically there are no improvements observed with estimated $a_{ph}(440)$ or $a_{cdm}(440)$ (Table 5). Analogous to the "error-free" cases, the $a_{cdm}(\lambda)$ at wavelengths longer than 440 nm are only improved to a limited degree from $R_{rs}$(UV+Vis). For $a_{ph}(\lambda)$, the degree of improvements in terms of RMSE and $\delta$ is even more limited.

Further, note that in the above tests the strong absorption in the ~300–400 nm range from mycosporine-like amino acids (MAAs) [e.g., *Ayoub et al.*, 2012; *Bricaud et al.*, 2010] is ignored due to a lack of remote sensing methods of knowing its existence and modeling its spectral variation. Because of the overlap spectral effect in the UV domain, the absorption of MAAs could reduce the benefit of $R_{rs}$(UV) in the retrieval of $S_{cdm}$ via the HOPE algorithm, and further limit the improvement in the retrieval of $a_{ph}(\lambda)$ and $a_{cdm}(\lambda)$.

## 5. Discussion

The composition and photochemistry of CDOM and detrital material in natural waters contribute to the large variability in their absorption spectral slope [*Carder et al.*, 1989; *Helms et al.*, 2008]. Variation of the spectral slope subsequently causes conspicuous divergence in the $R_{rs}$ spectra in the UV spectral region, while resulting in limited variability in the visible domain (Figures 1 and 2). The small $R_{rs}$ spectral differences in the visible domain identified in Figure 1 are close to the satellite measurement uncertainty of $R_{rs}$ (~0.0004 $sr^{-1}$ in the blue-green) over clear oceanic waters [*Gordon*, 1997; *Hu et al.*, 2013]. So it will be difficult to fully identify/separate the waters with highly resembling $R_{rs}$ spectra from each other (such as the cases shown in Figure 1) by only using the visible ocean color bands. Certainly, measurement errors and uncertainties have been embedded in the $R_{rs}$ spectra shown in Figure 1. Considering the fact that each pair of $R_{rs}$ spectra was measured by the same instrument in clear oceanic waters, the systematic errors should be minimal and would not be expected to contribute significantly to the differences in the UV domain (Table 1). Besides, each pair of $R_{rs}$ spectra is from waters of roughly the same and very low chlorophyll a concentrations (Table 1), thus errors due to self-shading [*Gordon and Ding*, 1992] should be negligible.

Our analyses suggest that the semianalytical retrieval of $S_{cdm}$ is considerably improved by adding $R_{rs}$ information in the UV bands in the inversion process (Tables 2 and 3). This finding has useful implications to present and future ocean color remote sensing. Unlike the hyperspectral UV-visible $R_{rs}$ data used in this study, the heritage and currently operational ocean color satellite sensors measure the water leaving radiance at a limited number of visible bands only. For example, the MODIS Aqua sensor images the global ocean at the wavelengths of 412, 443, 488, 531, 547, 667, and 683 nm (FWHM = ~10 nm). Due to a lack of information in the UV domain, these visible wavelengths alone cannot provide sufficient information required for an accurate construction of $R_{rs}$ spectrum in the UV and visible.

This lack of spectral information in UV may have impacted the inversion of $S_{cdm}$ from satellite ocean color remote sensing (Tables 2 and 3). In optical models, an often-adopted practice is to predict the $S_{cdm}$ as a function of $R_{rs}$ band ratios [e.g., *Lee et al*., 2009; *Wei and Lee*, 2015]. As previously discussed, however, the $R_{rs}$ band ratios in the visible domain may not fully account for the variability of the CDM absorption spectra, and large uncertainties may be resulted in the estimations of $S_{cdm}$ from such band ratios with $R_{rs}$ in the visible bands as inputs. A commonly used band-ratio algorithm for $S_{cdm}$ [*Lee et al*., 2009] is first tested here, which is defined as $S_{cdm} = 0.015 + 0.002/(0.6+R_{rs}(440)/R_{rs}(550))$. For the "error-free" evaluation data, the empirically derived $S_{cdm}$ is subject to an average error with $\delta = 20\%$. For the "error-disturbed" evaluation data, the band-ratio algorithm generates $S_{cdm}$ with $\delta = 23\%$. These are larger errors compared to the results shown in Tables 2 and 3, which are semianalytically inverted from UV-visible ocean color.

Simultaneous derivation of both CDM and phytoplankton absorption is an important task for satellite ocean color remote sensing [*Carder et al*., 1999; *Lee et al*., 2002; *Mouw et al*., 2013; *Smyth et al*., 2006]. *Wei and Lee* [2015] discussed the effects of including one UV wavelength into multiple-band ocean color algorithm on the separation of $a_{cdm}(\lambda)$ and $a_{ph}(\lambda)$. They reported the retrievals of $a_{cdm}(\lambda)$ can be improved to some degree with the addition of 380 nm wavelength, while more limited improvement is observed with the retrieval of $a_{ph}(\lambda)$. Based on the data set evaluated, the result further confirmed that the degree of improvements in $a_{ph}$ and $a_{cdm}$ retrievals from $R_{rs}$(UV+Vis) is limited. This is likely because that a reduction of error from 18% to 12% in the estimation of $S_{cdm}$ (Table 2) has a mild impact on the propagation of $a_{cdm}$ from shorter wavelength to longer wavelength. For instance, for a true $S_{cdm}$ value of 0.015 $nm^{-1}$, assuming the estimated $S_{cdm}$ from $R_{rs}$(UV+vis) as 0.0165 $nm^{-1}$ and 0.018 $nm^{-1}$ from $R_{rs}$(Vis), the propagation from $a_{cdm}(360)$ to $a_{cdm}(440)$ with the two estimated $S_{cdm}$ values differ by just ~12%.

The HOPE model adopted in this study has mechanistically explained the roles of UV wavelengths in retrieving $a_{cdm}(\lambda)$, $a_{ph}(\lambda)$ as well as the CDM spectral slope $S_{cdm}$. It does not require *a priori* knowledge of $S_{cdm}$. *Brando et al*. [2012] reported that the spectral slope $S_{cdm}$ may be retrieved from the $R_{rs}$ at MODIS bands. The adaptive semianalytical algorithm used therein required a predetermined ensemble of optically active constituents including the $S_{cdm}$ values. *Cao and Miller* [2015] proposed an empirical algorithm for retrieving CDOM absorption spectral information in the UV from visible ocean color bands. However, as any empirical algorithm their approach has limitations when applied to areas outside the training data set.

It is noted that, like in many other studies [*Bricaud et al*., 1981, 2010], a single spectral slope has been assumed here for the CDOM and CDM absorption coefficient in the UV and visible domain. Indeed, the wavelength-dependent spectral slopes for CDOM have been reported for various waters. Based on a large number of in situ CDOM spectra along U.S. coasts, *Twardowski et al*. [2004] found that those spectra in the visible range can be best described by a power-law function. *Reader and Miller* [2011] also reported that the single slope model could underestimate the CDOM absorption particularly at UV and shorter blue wavelengths. These studies have suggested a nonconstant, a.k.a., wavelength-dependent spectral slope, $S_{cdom}(\lambda)$. Generally $S_{cdom}(\lambda)$ has a decreasing trend with increasing wavelengths [also see *Swan et al*., 2013]. Such a nonconstant spectral slope model easily fits in the schemes as depicted by Figure 2, where the $R_{rs}$ spectral shapes are most sensitive to the $S_{cdom}(\lambda)$ in the UV domain and blue wavelengths. And inversion of such spectrally varying spectral slope $S_{cdom}(\lambda)$ should also be feasible as long as its spectral behavior can be appropriately characterized.

## 6. Conclusions

This study is motivated by field measurements of hyperspectral remote sensing reflectance spectra (360–700 nm) across a range of coastal and open ocean environments, showing that spectral variability in $R_{rs}$

increases by more than a factor of 4 in the UV region compared to the visible domain (difference of $R_{rs}$ $<$0.0005 sr$^{-1}$ in the visible increasing to $\sim$0.0023 sr$^{-1}$ in the UV). The mechanisms of the contrasting spectral features in the UV and visible domains are investigated through radiative transfer simulations. Because the CDM absorption is much stronger than the phytoplankton absorption in the UV domain (when absorption of MAAs is ignored), the change of the CDM absorption with a varying $S_{cdm}$ will significantly alter the shapes of $R_{rs}$ in the UV. In the visible domain, the impact of $S_{cdm}$ variation on $R_{rs}$ spectrum could be secondary because the contribution of phytoplankton absorption is generally stronger than that of CDM, at least for most oceanic waters. These observations suggest that the addition of UV bands into the ocean color inversions improve the retrievals of the spectral slope of the CDM absorption coefficient.

Using synthesized data sets, we assessed the semianalytically retried $S_{cdm}$ from the remote sensing reflectance. Our analyses indicate that inclusion of $R_{rs}$(UV) in the semianalytical inversion process can considerably increase the accuracy of $S_{cdm}$ retrievals, at least for waters tested in this study. Although the degree of improvements may be related to the range of $a_{cdm}$(440) values, the study has confirmed the advantages of including $R_{rs}$(UV) in the retrievals for $S_{cdm}$. But, the degree of improvements in the retrievals of $a_{ph}(\lambda)$ and $a_{cdm}(\lambda)$ by including UV wavelengths in the inversions are actually limited, at least for the data set evaluated here.

This study on the roles of UV wavelengths in deriving CDM spectral slopes, and the subsequent impact on the decomposition of absorption coefficients into phytoplankton and CDM absorption highlights the necessity for accurate measurements of $R_{rs}$(UV) from space. It supports the recommendation of including spectral bands in the UV wavelengths in the next generation of satellite ocean color sensors, as such information could be also very useful for the remote sensing of aerosols and its correction in ocean color remote sensing.

**Acknowledgments**
Financial support by the **National Aeronautics and Space Administration (NASA) Ocean Biology and Biogeochemistry and Water and Energy Cycle Programs**, the **GEO-CAPE project, and the National Oceanic and Atmospheric Administration (NOAA)** JPSS VIIRS Ocean Color Cal/Val Project is greatly appreciated. The $R_{rs}$ data in the North Pacific Gyre were collected by Marlon Lewis at the Dalhousie University. We thank Emmanuel Boss and an anonymous reviewer for comments and suggestions, which have improved the manuscript.

## References

Antoine, D., F. d'Ortenzio, S. B. Hooker, G. Bécu, B. Gentili, D. Tailliez, and A. J. Scott (2008), Assessment of uncertainty in the ocean reflectance determined by three satellite ocean color sensors (MERIS, SeaWiFS and MODIS-A) at an offshore site in the Mediterranean Sea (BOUSSOLE project), *J. Geophys. Res.*, *113*, C07013, doi:10.1029/2007JC004472.

Aurin, D., and A. Mannino (2012), A database for developing global ocean color algorithms for colored dissolved organic material, CDOM spectral slope, and dissolved organic carbon, paper presented at Ocean Optics XXI, The Oceanography Society, Glasgow, U. K.

Austin, R. W. (1974), The remote sensing of spectral radiance from below the ocean surface, in *Optical Aspects of Oceanography*, edited by N. G. Jerlov and E. Steemann Nielsen, pp. 317–344, Academic, N. Y.

Ayoub, L. M., P. Hallock, P. G. Coble, and S. S. Bell (2012), MAA-like absorbing substances in Florida Keys phytoplankton vary with distance from shore and CDOM: Implications for coral reefs, *J. Exp. Mar. Biol. Ecol.*, *420–421*, 91–98, doi:10.1016/j.jembe.2012.03.026.

Babin, M., D. Stramski, G. M. Ferrari, H. Claustre, A. Bricaud, G. Obolensky, and N. Hoepffner (2003), Variations in the light absorption coefficients of phytoplankton, nonalgal particles, and dissolved organic matter in coastal waters around Europe, *J. Geophys. Res.*, *108*(4), 3211, doi:10.1029/2001JC000882.

Binding, C. E., J. H. Jerome, R. P. Bukata, and W. G. Booty (2008), Spectral absorption properties of dissolved and particulate matter in Lake Erie, *Remote Sens. Environ.*, *112*(4), 1702–1711, doi:10.1016/j.rse.2007.08.017.

Boss, E., W. S. Pegau, J. R. V. Zaneveld, and A. H. Barnard (2001), Spatial and temporal variability of absorption by dissolved material at a continental shelf, *J. Geophys. Res.*, *106*(C5), 9499–9507, doi:10.1029/2000JC900008.

Brando, V. E., A. G. Dekker, Y. J. Park, and T. Schroeder (2012), Adaptive semianalytical inversion of ocean color radiometry in optically complex waters, *Appl. Opt.*, *51*(15), 2808–2833, doi:10.1364/AO.51.002808.

Bricaud, A., A. Morel, and L. Prieur (1981), Absorption by dissolved organic matter of the sea (yellow substance) in the UV and visible domains, *Limnol. Oceanogr.*, *26*(1), 43–53.

Bricaud, A., M. Babin, A. Morel, and H. Claustre (1995), Variability in the chlorophyll-specific absorption coefficients of natural phytoplankton: Analysis and parameterization, *J. Geophys. Res.*, *100*(C7), 13,321–13,332, doi:10.1029/95JC00463.

Bricaud, A., A. Morel, M. Babin, K. Allali, and H. Claustre (1998), Variations of light absorption by suspended particles with chlorophyll a concentration in oceanic (case 1) waters: Analysis and implications for bio-optical models, *J. Geophys. Res.*, *103*(C13), 31,033–31,044, doi:10.1029/98JC02712.

Bricaud, A., M. Babin, H. Claustre, J. Ras, and F. Tieche (2010), Light absorption properties and absorption budget of Southeast Pacific waters, *J. Geophys. Res.*, *115*, C08009, doi:10.1029/2009JC005517.

Byrd, R. H., M. E. Hribar, and J. Nocedal (1999), An interior point algorithm for large-scale nonlinear programming, *SIAM J. Optim.*, *9*(4), 877–900.

Cao, F., and W. L. Miller (2015), A new algorithm to retrieve chromophoric dissolved organic matter (CDOM) absorption spectra in the UV from ocean color, *J. Geophys. Res. Oceans*, *120*, 496–516, doi:10.1002/2014JC010241.

Carder, K. L., R. G. Steward, G. R. Harvey, and P. B. Ortner (1989), Marine humic and fulvic acids: Their effects on remote sensing of ocean chlorophyll, *Limnol. Oceanogr.*, *34*, 68–81.

Carder, K. L., S. K. Hawes, K. A. Baker, R. C. Smith, R. G. Steward, and B. G. Mitchell (1991), Reflectance model for quantifying chlorophyll a in the presence of productivity degradation products, *J. Geophys. Res.*, *96*(C11), 20,599–20,611, doi:10.1029/91JC02117.

Carder, K. L., F. R. Chen, Z. P. Lee, S. K. Hawes, and D. Kamykowski (1999), Semianalytic moderate-resolution imaging spectrometer algorithms for chlorophyll-a and absorption with bio-optical domains based on nitrate-depletion temperatures, *J. Geophys. Res.*, *104*(C3), 5403–5421, doi:10.1029/1998JC900082.

Chin, Y.-P., G. Aiken, and E. O'Loughlin (1994), Molecular weight, polydispersity, and spectroscopic properties of aquatic humic substances, *Environ. Sci. Technol.*, *28*(11), 1853–1858, doi:10.1021/es00060a015.
Conmy, R. N., P. G. Coble, J. P. Cannizzaro, and C. A. Heil (2009), Influence of extreme strom events on West Florida Shelf CDOM distributions, *J. Geophys. Res.*, *114*, G00F04, doi:10.1029/2009JG000981.
Cullen, J. J., and P. J. Neale (1994), Ultraviolet radiation, ozone depletion, and marine photosynthesis, *Photosynth. Res.*, *39*(3), 303–320.
D'Sa, E. J., and R. L. Miller (2003), Bio-optical properties in waters influenced by the Mississippi River during low flow conditions, *Remote Sens. Environ.*, *84*(4), 538–549, doi:10.1016/S0034-4257(02)00163-3.
Del Castillo, C. E., and R. L. Miller (2008), On the use of ocean color remote sensing to measure the transport of dissolved organic carbon by the Mississippi River Plume, *Remote Sens. Environ.*, *112*(3), 836–844.
Del Castillo, C. E., and R. L. Miller (2011), Horizontal and vertical distributions of colored dissolved organic matter during the Southern Ocean Gas Exchange Experiment, *J. Geophys. Res.*, *116*, C00F07, doi:10.1029/2010JC006781.
Del Castillo, C. E., et al. (2012), Pre-aerosol, clouds, and ocean ecosystem (PACE) mission science definition team report, NASA, Washington, D. C. [Available at http://decadal.gsfc.nasa.gov/pace_documentation/PACE_SDT_Report_final.pdf.]
Fichot, C. G., and R. Benner (2012), The spectral slope coefficient of chromophoric dissolved organic matter ($S_{275\text{-}295}$) as a tracer of terrigenous dissolved organic carbon in river-influenced ocean margins, *Limnol. Oceanogr.*, *57*(5), 1453–1466.
Fishman, J., et al. (2012), The United States' next generation of atmospheric composition and coastal ecosystem measurements: NASA's geostationary coastal and air pollution events (GEO-CAPE) mission, *Bull. Am. Meteorol. Soc.*, *93*(10), 1547–1566, doi:10.1175/BAMS-D-11-00201.1.
Gordon, H. R. (1997), Atmospheric correction of ocean color imagery in the Earth observing system era, *J. Geophys. Res.*, *102*(D), 17,081–17,106, doi:10.1029/96JD02443.
Gordon, H. R., and K. Ding (1992), Self-shading of in-water optical instruments, *Limnol. Oceanogr.*, *37*(3), 491–500.
Gordon, H. R., and A. Morel (1983), *Remote Assessment of Ocean Color for Interpretation of Satellite Visible Imagery: A Review*, 44 pp., Springer, N. Y.
Gordon, H. R., and M. Wang (1994), Retrieval of water-leaving radiance and aerosol optical thickness over the oceans with SeaWiFS: A preliminary algorithm, *Appl. Opt.*, *33*(3), 443–452.
Gordon, H. R., O. B. Brown, R. H. Evans, J. W. Brown, R. C. Smith, K. S. Baker, and D. K. Clark (1988), A semianalytic radiance model of ocean color, *J. Geophys. Res.*, *93*(D9), 10,909–10,924, doi:10.1029/JD093iD09p10909.
Helms, J. R., A. Stubbins, J. D. Ritchie, E. C. Minor, D. J. Kieber, and K. Mopper (2008), Absorption spectral slopes and slope ratios as indicators of molecular weight, source, and photobleaching of chromophoric dissolved organic matter, *Limnol. Oceanogr.*, *53*(3), 955–969.
Hernes, P. J., and R. Benner (2003), Photochemical and microbial degradation of dissolved lignin phenols: Implications for the fate of terrigenous dissolved organic matter in marine environments, *J. Geophys. Res.*, *108*(C9), 3291, doi:10.1029/2002JC001421.
Hu, C., L. Feng, and Z. P. Lee (2013), Uncertainties of SeaWiFS and MODIS remote sensing reflectance: Implications from clear water measurements, *Remote Sens. Environ.*, *133*(2), 168–182.
Huot, Y., A. Morel, M. S. Twardowski, D. Stramski, and R. A. Reynolds (2008), Particle optical backscattering along a chlorophyll gradient in the upper layer of the eastern South Pacific Ocean, *Biogeosciences*, *5*, 495–507.
IOCCG (2006), *Remote Sensing of Inherent Optical Properties: Fundamentals, Tests of Algorithms, and Applications*, 126 pp., Dartmouth, Nova Scotia, Canada.
Jerlov, N. G. (1976), *Marine Optics*, 231 pp., Elsevier Sci., Amsterdam, Netherlands.
Johannessen, S. C., W. L. Miller, and J. J. Cullen (2003), Calculation of UV attenuation and colored dissolved organic matter absorption spectra from measurements of ocean color, *J. Geophys. Res.*, *108*(C9), 3301, doi:10.1029/2000JC000514.
Lee, Z. P., K. L. Carder, C. D. Mobley, R. G. Steward, and J. S. Patch (1999), Hyperspectral remote sensing for shallow waters: 2. Deriving bottom depths and water properties by optimization, *Appl. Opt.*, *38*(18), 3831–3843.
Lee, Z. P., K. L. Carder, and R. Arnone (2002), Deriving inherent optical properties from water color: A multi-band quasi-analytical algorithm for optically deep waters, *Appl. Opt.*, *41*(27), 5755–5772.
Lee, Z. P., K. L. Carder, and K. P. Du (2004), Effects of molecular and particle scatterings on model parameters for remote-sensing reflectance, *Appl. Opt.*, *43*(25), 4957–4964.
Lee, Z. P., B. Lubac, J. Werdell, and R. Arnone (2009), An update of the quasi-analytical algorithm (QAA_v5), International Ocean-Colour Coordinating Group (IOCCG), Dartmouth, Nova Scotia, Canada. [Available at http://www.ioccg.org/groups/Software_OCA/QAA_v5.pdf.]
Lee, Z. P., S. Shang, C. Hu, M. Lewis, R. Arnone, Y. Li, and B. Lubac (2010), Time series of bio-optical properties in a subtropical gyre: Implications for the evaluation of inter-annual trends of biogeochemical properties, *J. Geophys. Res.*, *115*, C09012, doi:10.1029/2009JC005865.
Lee, Z. P., N. Pahlevan, Y.-H. Ahn, S. Greb, and D. O'Donnell (2013), Robust approach to directly measuring water-leaving radiance in the field, *Appl. Opt.*, *52*(8), 1693–1701.
Lee, Z. P., J. Wei, K. Voss, M. Lewis, A. Bricaud, and Y. Huot (2015), Hyperspectral absorption coefficient of "pure" seawater in the range of 350-550 nm inverted from remote sensing reflectance, *Appl. Opt.*, *54*(3), 546–558.
Lesser, M. P., and J. H. Farrell (2004), Exposure to solar radiation increases damage to both host tissues and algal symbionts of corals during thermal stress, *Coral Reefs*, *23*, 367–377.
Loisel, H., and D. Stramski (2000), Estimation of the inherent optical properties of natural waters from the irradiance attenuation coefficient and reflectance in the presence of Raman scattering, *Appl. Opt.*, *39*(18), 3001–3011.
Mannino, A., M. E. Russ, and S. B. Hooker (2008), Algorithm development and validation for satellite-derived distributions of DOC and CDOM in the US Middle Atlantic Bight, *J. Geophys. Res.*, *113*, C07051, doi:10.1029/2007JC004493.
Mannino, A., M. G. Novak, S. B. Hooker, K. Hyde, and D. Aurin (2014), Algorithm development and validation of CDOM properties for estuarine and continental shelf waters along the northeastern U.S. coast, *Remote Sens. Environ.*, *152*, 576–602, doi:10.1016/j.rse.2014.06.027.
Maritorena, S., D. A. Siegel, and A. R. Peterson (2002), Optimization of a semianalytical ocean color model for global-scale applications, *Appl. Opt.*, *41*(15), 2705–2714.
Matsuoka, A., S. B. Hooker, A. Bricaud, B. Gentili, and M. Babin (2013), Estimating absorption coefficients of colored dissolved organic matter (CDOM) using a semi-analytical algorithm for southern Beaufort Sea waters: Application to deriving concentrations of dissolved organic carbon from space, *Biogeosciences*, *10*, 917–927, doi:10.5194/bg-10-917-2013.
Mobley, C. D. (1994), *Light and Water: Radiative Transfer in Natural Waters*, 592 pp., Academic, San Diego, Calif.
Mobley, C. D., and L. K. Sundman (2008), *Hydrolight 5 and Ecolight 5 User's Guide*, 99 pp., Sequoia Sci., Inc., Bellevue, Wash.
Morel, A. (1974), Optical properties of pure water and pure sea water, in *Optical Aspects of Oceanography*, edited by N. G. Jerlov and E. Steemann Nielsen, 494 pp., Academic, N. Y.
Morel, A., and B. Gentili (2010), The most oligotrophic subtropical zones of the global oceans: Similarities and differences in terms of chlorophyll and yellow substance, *Biogeosciences*, *7*, 3139–3151.

Mouw, C. B., H. Chen, G. A. McKinley, S. Effler, D. O'Donnell, M. G. Perkins, and C. Strait (2013), Evaluation and optimization of bio-optical inversion algorithms for remote sensing of Lake Superior's optical properties, *J. Geophys. Res. Oceans*, *118*, 1696–1714, doi:10.1002/jgrc.20139.

Nelson, N. B., and D. A. Siegel (2002), Chromophoric DOM in the open ocean, in *Biogeochemistry of Marine Dissolved Organic Matter*, edited by D. A. Hansell and C. A. Carlson, pp. 547–578, Elsevier Sci., San Diego, Calif.

Nelson, N. B., C. A. Carlson, and D. K. Steinberg (2004), Production of chromophoric dissolved organic matter by Sargasso Sea microbes, *Mar. Chem.*, *89*(1–4), 273–287, doi:10.1016/j.marchem.2004.02.017.

Nelson, N. B., D. A. Siegel, C. A. Carlson, C. Swan, W. M. Smethie Jr, and S. Khatiwala (2007), Hydrography of chromophoric dissolved organic matter in the North Atlantic, *Deep Sea Res., Part I*, *54*(5), 710–731, doi:10.1016/j.dsr.2007.02.006.

Pan, X., A. Mannino, M. E. Russ, and S. B. Hooker (2008), Remote sensing of the absorption coefficients and chlorophyll a concentration in the United States southern Middle Atlantic Bight from SeaWiFS and MODIS-Aqua, *J. Geophys. Res.*, *113*, C11022, doi:10.1029/2008JC004852.

Pope, R. M., and E. S. Fry (1997), Absorption spectrum (380-700 nm) of pure water. II. Integrating cavity measurements, *Appl. Opt.*, *36*(33), 8710–8723.

Preisendorfer, R. W. (1976), *Hydrologic Optics*, 218 pp., U.S. Gov. Print. Off., Honolulu, Hawaii.

Reader, H. E., and W. L. Miller (2011), Effect of estimations of ultraviolet absorption spectra of chromophoric dissolved organic matter on the uncertainty of photochemical production calculations, *J. Geophys. Res.*, *116*, C08002, doi:10.1029/2010JC006823.

Roesler, C. S., M. J. Perry, and K. L. Carder (1989), Modeling in situ phytoplankton absorption from total absorption spectra in productive inland marine waters, *Limnol. Oceanogr.*, *34*(8), 1510–1523, doi:10.2307/2837036.

Shank, G. C., R. Lee, A. Vähätalo, R. G. Zepp, and E. Bartels (2010), Production of chromophoric dissolved organic matter from mangrove leaf litter and floating Sargassum colonies, *Mar. Chem.*, *119*(1–4), 172–181, doi:10.1016/j.marchem.2010.02.002.

Shick, J. M., M. P. Lesser, and P. L. Jokiel (1996), Effects of ultraviolet radiation on corals and other coral reef organisms, *Global Change Biol.*, *2*, 527–545.

Siegel, D. A., S. Maritorena, N. B. Nelson, D. A. Hansell, and M. Lorenzi-Kayser (2002), Global distribution and dynamics of colored dissolved and detrital organic materials, *J. Geophys. Res.*, *107*(C12), 3228, doi:10.1029/2001JC000965.

Siegel, D. A., S. Maritorena, N. B. Nelson, M. J. Behrenfeld, and C. R. McClain (2005), Colored dissolved organic matter and its influence on the satellite-based characterization of the ocean biosphere, *Geophys. Res. Lett.*, *32*, L20605, doi:10.1029/2005GL024310.

Smyth, T. J., G. F. Moore, T. Hirata, and J. Aiken (2006), Semianalytical model for the derivation of ocean color inherent optical properties: Description, implementation, and performance assessment, *Appl. Opt.*, *45*(31), 8116–8131.

Steinberg, D. K., N. B. Nelson, C. A. Carlson, and A. C. Prusak (2004), Production of chlromophoric dissolved organic matter (CDOM) in the open ocean by zooplankton and the colonial cyanobacterium Trichodesmium spp., *Mar. Ecol. Prog. Ser.*, *267*, 45–56.

Swan, C. M., N. B. Nelson, D. A. Siegel, and E. A. Fields (2013), A model for remote estimation of ultraviolet absorption by chromophoric dissolved organic matter based on the global distribution of spectral slope, *Remote Sens. Environ.*, *136*, 277–285.

Twardowski, M. S., and P. L. Donaghay (2002), Photobleaching of aquatic dissolved materials: Absorption removal, spectral alteration, and their interrelationship, *J. Geophys. Res.*, *107*(C8), 3091, doi:10.1029/1999JC000281.

Twardowski, M. S., E. S. Boss, J. M. Sullivan, and P. L. Donaghay (2004), Modeling the spectral shape of absorption by chromophoric dissolved organic matter, *Mar. Chem.*, *89*(1–4), 69–88.

Tzortziou, M., J. R. Herman, C. L. Gallegos, P. J. Neale, A. Subramaniam, L. W. Harding, and Z. Ahmad (2006), Bio-optics of the Chesapeake Bay from measurements and radiative transfer closure, *Estuarine Coastal Shelf Sci.*, *68*(1–2), 348–362.

Tzortziou, M., P. J. Neale, C. L. Osburn, J. P. Megonigal, N. Maie, and R. JaffÉ (2008), Tidal marshes as a source of optically and chemically distinctive colored dissolved organic matter in the Chesapeake Bay, *Limnol. Oceanogr.*, *53*(1), 148–159, doi:10.4319/lo.2008.53.1.0148.

Wang, M., S. Son, and W. Shi (2009), Evaluation of MODIS SWIR and NIR-SWIR atmospheric correction algorithm using SeaBASS data, *Remote Sens. Environ.*, *113*, 635–644.

Wang, X., R. F. Chen, and G. B. Gardner (2004), Sources and transport of dissolved and particulate organic carbon in the Mississippi River estuary and adjacent coastal waters of the northern Gulf of Mexico, *Mar. Chem.*, *89*, 241–256.

Wei, J., and Z. P. Lee (2015), Retrieval of phytoplankton and color detrital matter absorption coefficients with remote sensing reflectance in an ultraviolet band, *Appl. Opt.*, *54*(4), 636–649.

Wei, J., Z. P. Lee, M. Lewis, N. Pahlevan, M. Ondrusek, and R. Armstrong (2015), Radiance transmittance measured at the ocean surface, *Opt. Express*, *23*(9), 11,826–11,837.

Zheng, G., D. Stramski, and R. A. Reynolds (2014), Evaluation of the Quasi-Analytical Algorithm for estimating the inherent optical properties of seawater from ocean color: Comparison of Arctic and lower-latitude waters, *Remote Sens. Environ.*, *155*, 194–209, doi:10.1016/j.rse.2014.08.020.